Close-packed assemblies of discrete tiny silver nanoparticles on triangular gold nanoplates as a high performance SERS probe†

Youju Huang,‡*[a] Palanisamy Kannan,‡[b] Lei Zhang,[a] Yun Rong,[a] Liwei Dai,[a] Rongqin Huang[c] and Tao Chen*[a]

Bimetallic nanocatalysts often display enhanced physical and chemical properties compared to those of their monometallic counterparts. Herein, we introduce a simple method to fabricate an island like array of tiny Ag nanoparticles bounded on triangular Au nanoplates as the surface-enhanced Raman scattering (SERS) substrate. The surface morphology of the synthesized nanoparticles was characterized *via* field emission scanning electron microscopy (FE-SEM), and atomic force microscopy (AFM). Rhodamine 6G (R6G) is used as a model analyte to evaluate the performance of the tiny Ag nanoparticle bounded triangular Au nanoplates as a SERS-active substrate and validate the SERS effect. The fabricated SERS substrate showed drastically enhanced intensity with a SERS enhancement factor as high as 10^7, which is enough to detect a single molecule, and excellent reproducibility (less than ±5%) of the signal intensity. This is because of the island-like tiny Ag nanoparticle bounded triangular Au nanoplates and their large number of "hot spots". This substrate could also be used for label-free immunoassays, biosensing, and nanoscale optical antennas and light sources.

1. Introduction

Nanostructured noble metal particles have received considerable interest in recent years due to their fascinating optical, electronic, and catalytic properties.[1–7] Of course, the synthesis of distinct anisotropic morphologies of noble metal nanostructures is recently attracting the significant attention of chemists and materials scientists.[8–10] The inherent properties of these noble metal nanostructures can be tuned by controlling their size and shape.[11–14] Significant enrichment of optical and catalytic properties can be achieved by tuning their shape than the size because nanocrystalline surfaces have different surface atom densities and electronic structures.[15] Thus, the properties of nanostructures having remarkable shape may significantly differ from those of common spherical shapes. Such anisotropic noble nanoparticles have enormous potential applications in bio-sensors and bio-diagnosis technologies.[16–18]

Plasmonic metal nanoparticles find wide applications in bioanalytical chemistry for detection, discrimination, and diagnosis of biological probes.[19–22] One of the most common techniques hereby is surface-enhanced Raman scattering (SERS) where the resonant coupling of light with the particle's surface plasmons is used to enhance the Raman signal of molecules in close vicinity of the particle surface. The derived vibrational pattern provides the molecular fingerprint information of a target molecule with a high degree of sensitivity and low detection limits; hence, SERS spectroscopy is able to discriminate the different types of biomolecules or microorganisms.[23–25] When compared to conventional fluorescence detection techniques, SERS also possesses other intrinsic benefits, such as reduced photobleaching, narrow spectroscopic bands for detecting multiple species, and the ability to operate over a wide excitation wavelength range.[26] The SERS effects are generally observed in metal substrates that are especially coarse on a micro/nanoscale.[27,28] Thus, much effort has been devoted to the design and fabrication of highly sensitive and reproducible SERS-active noble metal substrates. Nanostructures employed in previous studies include nanoparticle arrays,[29–33] aggregated nanoparticles,[34,35] nanostructured metallic films,[36,37] and metal nanoshells.[38]

Among the various nanomaterials, colloidal gold (Au) and silver (Ag) nanoparticles are of special interest in SERS as a substrate,[39–42] mainly because they strongly scatter light and their optical properties depend on the size, shape, and aggregation state.[1] Because dramatic enhancement in the scattering

[a]*Division of Polymer and Composite Materials, Ningbo Institute of Material Technology and Engineering, Chinese Academy of Science, 1219 Zhongguan West Road, Ningbo 315201, China. E-mail: yjhuang@nimte.ac.cn; tao.chen@nimte.ac.cn*

[b]*Singapore Centre on Environmental Life Science Engineering (SCELSE), Nanyang Technological University, Singapore*

[c]*Key Laboratory of Smart Drug Delivery, Ministry of Education (Fudan University), Shanghai 201203, China*

can be observed for the molecules adsorbed on the nanostructured particles, single molecule spectroscopy is possible by SERS.[43,44] More important is several examples have been demonstrated in which bimetallic nanoparticles have superior catalytic activity relative to their monometallic counterparts due to the synergism between the metal components.[45–47] Basically, a volcano-type association between composition and catalytic activity has been reported for various bimetallic systems and assigned to electronic and/or geometric effects. In this report, we describe a simple approach for the synthesis of close-packed assemblies of discrete tiny Ag nanoparticles on triangular Au nanoplates, and its high performance SERS analysis towards rhodamine 6G as the probe molecule for the first time.

2. Experimental section

2.1. Materials and instruments

Cetyltrimethylammonium bromide (CTAB), hydrogen tetrachloroaurate(III) trihydrate ($HAuCl_4 \cdot 3H_2O$), silver nitrate ($AgNO_3$), ascorbic acid (AA) and sodium citrate were purchased from Sigma-Aldrich. All other reagents were used as received. The UV-vis-NIR absorption spectra were collected from 400 to 1400 nm on a spectrophotometer (Varian Cary 5000). Field-emission scanning electron microscopy (FE-SEM) was performed on the JEOL instrument (JSM-6700F) at an acceleration voltage of 5 kV and a working distance between 7 and 8 mm. The specimens were prepared by dropping 3 μL of the colloidal nanoparticles solution on a silicon (Si) wafer substrate. The AFM images were obtained in air from an Asylum Research MFP-3D AFM system conducted in tapping mode using a super sharp silicon AFM tip purchased from NanoWorld. Raman spectra were collected using a Renishaw inVia confocal Raman spectrometer mounted on a Leica microscope with 50× objective lens (NA = 0.80) in the range of 100–2000 cm^{-1} with one accumulation and 25 s exposure time. A 633 nm wavelength HeNe laser (85 μW at the sample surface) was used to excite the sample.

2.2. Synthesis of triangular Au nanoplates

Triangular Au nanoplates were synthesized according to our previous report.[8] Briefly, 0.5 mL of 20 mM $HAuCl_4$ solution was mixed with 1 mL of 10 mM sodium citrate and 36.5 mL water. Then 1.0 mL of 0.1 M $NaBH_4$ was added to the mixed solution with vigorous stirring for 2 min. The obtained solution turned yellowish pink and was kept at room temperature for at least 4 hours before use. Next, growth solution was prepared by mixing 108 mL of 0.025 M CTAB solution, 1.5 mL of 0.02 M $HAuCl_4$, and 0.6 mL of 0.1 M NaOH, 54 μL of 0.1 M KI and 0.6 mL of 0.1 M ascorbic acid. In order to favour the formation of uniform TAuNPTs, Au seeds were fast handled during multiple-step growth. First, 0.1 mL of seeds solution was added into 0.9 mL of growth solution with gentle shaking for 3 s, and then immediately, 9 mL of growth solution was added. After 3 s of gentle shaking, the mixed solution was added into another 92 mL of growth solution in a glass beaker. After half an hour, the solution turned deep purple, indicating the formation of AuNPs. The solution was then kept without any alteration for 24 hours, allowing attachment of triangular Au nanoplates to the walls of the beaker. Then, the solution was gently poured out and 20 mL of 0.025 M CTAB solution was added to re-disperse TAuNPTs. The solution is green with a strong absorption in the NIR region.

2.3. Synthesis of tiny Ag nanoparticles on triangular Au nanoplates

Four aliquots (2 mL each) of CTAB-capped triangular Au nanoplates were added into four plastic tubes, and label as A, B, C, and D. Then, 0.2, 0.5, 1.0 and 2.0 mL of $AgNO_3$ (0.001 M) were subsequently added into the four labelled aliquots tubes (A–D), respectively. After the sonication for 2 min, 0.1, 0.25, 0.5 and 1.0 mL of ascorbic acid solutions (0.01 M) were added into the four respective labelled tubes. The solutions were then kept at 65 °C in a water bath for 4 h, which results tiny Ag nanoparticles were successfully grown on the triangular Au nanoplates.

2.4. SERS substrate preparation

3 μL of as-prepared tiny Ag nanoparticles on triangular Au nanoplates slowly dropped on a cleaned Si-wafer surface and dried in a nitrogen atmosphere for 2 h to form a uniform SERS active substrate. The 5 μL of (0.1 mM) R6G molecule was further dropped on the above substrate and allowed 2 more hours drying under nitrogen atmosphere for SERS analysis.

3. Results and discussion

3.1. Characterisation of nanoparticles

Size, morphology and topography of the synthesized triangular Au nanoplates and tiny Ag nanoparticles bounded triangular Au nanoplates were characterized by FE-SEM, and AFM techniques. The SEM image in Fig. 1a confirms the high uniformity of the obtained triangular nanoplates, with a few distorted plates, and rarely one or two spherical AuNPs found in the sample. The average edge length of the synthesized triangular Au nanoplates is 140 ± 5 nm, and the monodispersity in edge length is significantly improved (relative standard deviation (RSD) of ~5.1%) compared with those in previous reports.[48,49] Atomic force microscopy (AFM) image is showing island like triangular Au nanoplates confirms that their lateral surfaces are atomically

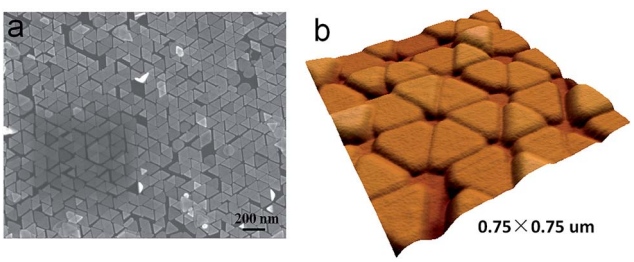

Fig. 1 (a) FE-SEM image of triangular Au nanoplates obtained under optimized conditions (5 s time interval and 0.025 M of CTAB); 3D tapping mode AFM image of triangular Au nanoplates. (b) The scan size for the 3D AFM image is 0.5 × 0.5 μm.

flat with a uniform thickness of 8.0 ± 0.5 nm (from its height profile).[8] Further, the truncation of edges in the triangular Au nanoplates is clearly evident in the AFM image. In addition, it was seen that a few irregular Au triangles covered the surfaces. These were small, typically measuring just ~30 nm in width, in accordance with the critical concentration of CTAB.

The UV-vis-NIR absorption spectrum of the sample obtained under optimized conditions is shown in Fig. 2. Two absorption peaks at 880 nm and 1350 nm in the spectrum correspond to the in-plate quadrupole mode and in-plane dipole mode plasmon resonances of the triangular Au nanoplates.[48] It is worth noting that the peak at 1350 nm is significantly stronger than those in the previous report,[50] and no peak is observed at 500–600 nm, indicating an exceptionally high purity of triangular Au nanoplates suspension (Fig. 2a). Hereafter, triangular Au nanoplates is added to the tiny Ag nanoparticle growth solution, and we noticed the changes in the UV-vis-NIR absorption spectrum, and FE-SEM analysis.

Initial addition of growth solution $AgNO_3$ (0.2 mL), and AA (0.1 mL) into the triangular Au nanoplates results that UV-vis-NIR absorption spectrum was blue shifted, and broadened at 1250 nm, which means tiny Ag nanoparticles were started to grow on the surface of triangular Au nanoplates (Fig. 2b). As can be seen in the corresponding FE-SEM image is shown in Fig. 3a indicating few dots of tiny Ag nanoparticles were obviously found on the triangular Au nanoplates. In the next step, subsequent increase of both $AgNO_3$, and AA (0.5, and 0.25 mL), their UV-vis-NIR absorption spectrum further blue shifted at 1050 nm (Fig. 2c), produced low density of tiny Ag nanoparticles on triangular nanoplates surfaces (Fig. 3b). Importantly, a distinguished small appeared at 690 nm was corresponding to the characteristic surface plasmon band for the spherical shaped tiny Ag nanoparticles (Fig. 2c).[1] Further, two more steps increase (volume) of growth solution ($AgNO_3$: AA = 1 : 0.5 mL, and 2 : 1 mL) yielded high density (Fig. 3c), as well as island like tiny Ag nanoparticles on the surface of triangular Au nanoplates

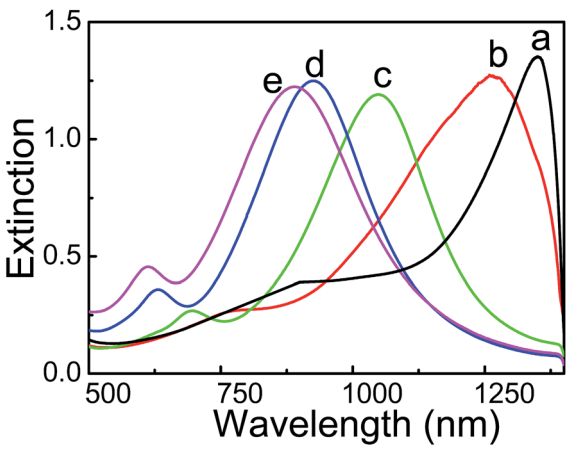

Fig. 2 UV-vis-NIR absorption spectra of triangular Au nanoplates obtained before (a) and after in different volumes of $AgNO_3$: AA growth solution in the respective tubes 0.2 : 0.1 mL (b), 0.5 : 0.25 mL (c), 1 : 0.5 mL (d), and 2 : 1 mL (e) for growing tiny AgNPs.

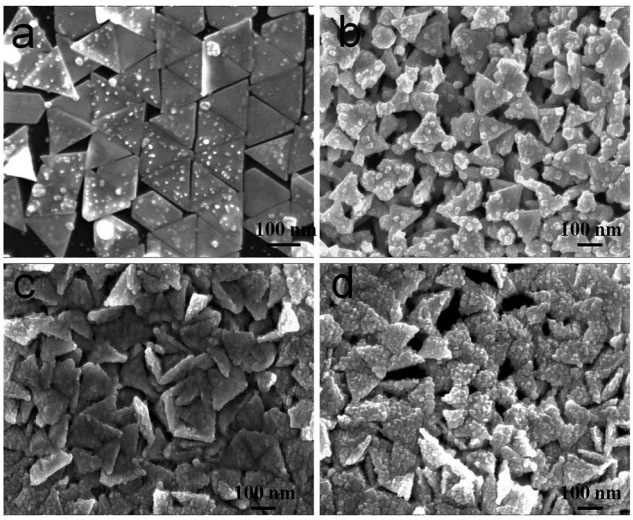

Fig. 3 Representative FE-SEM images of tiny Ag nanoparticles grown on triangular Au nanoplates at different volume ratio's of growth solution: 0.2 : 0.1 mL (a), 0.5 : 0.25 mL (b), 1 : 0.5 mL (c), and 2 : 1 mL (d), respectively. The scale bars represent 100 nm.

(Fig. 3d), and the corresponding UV-vis-NIR absorption spectrum was confirmed the formation tiny Ag nanoparticles (Fig. 2d and e). Initially, the formation of few tiny AgNPs is due to slow reduction of $AgNO_3$ by AA.[51] AA is naturally occurring biological compound, and showed mild reducing character to reduce Ag (or Au) salt. However, then we increased the concentration of AA up to 1 mL resulted the high density of tiny AgNPs deposited on Au nanotriangles.

3.2. SERS analysis of R6G molecule

It is well known that the high performance SERS correlates with number of hot spots available in the substrate. Metal nanostructures are also tremendously useful in various spectroscopic techniques, including surface enhanced Raman scattering (SERS)[52] due to the strong electric field generated on metal nanoparticles upon light illumination and the formation of "hot spots". The "hot spots" can contribute to the enhancement of the Raman signal were usually located at the gaps and the corners of metal nanoparticles (Scheme 1). These properties can be further influenced and enhanced by bringing two or more metal nanoparticles together.[53,54] The best example is the dramatic enhancement in the SERS signal at nanoparticle

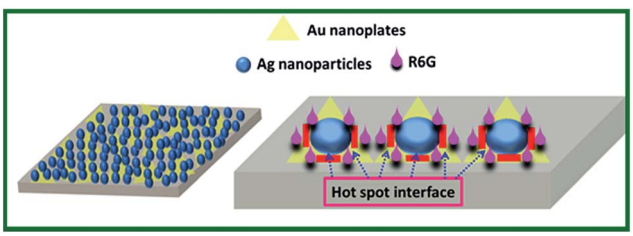

Scheme 1 The schematic representation of SERS substrate, and the location of "hot spots".

junctions, which enables the detection of single molecules.[55–57] In this work, we prepared tiny Ag nanoparticles bounded triangular Au nanoplates for active SERS substrate, considering that the Ag nanomaterials have excellent SERS properties. Rhodamine 6G (R6G) was used as the probe molecule for the SERS measurement (Fig. 4). We studied SERS signals from bare Si wafer (a), the representative nanoparticles samples were shown in Fig. 1a, and 3a–d, such as (b) triangular Au nanoplates, triangular Au nanoplates with different volumes of tiny Ag nanoparticles growth solution ($AgNO_3$: AA), 0.2 : 0.1 mL (c), 0.5 : 0.25 mL (d), 1 : 0.5 mL (e), and 2 : 1 mL (f). All of these nanostructures are supported on Si substrates each measuring 0.5 × 0.5 cm^2.

R6G was dissolved in ethanol (0.1 mM) and 5 μL of the solution was dropped on the different substrates before obtaining the signals using a 633 nm HeNe laser source with one accumulation and 10 s exposure time. The SERS spectra of R6G on bare Si wafer shown ill-defined Raman bands, however the strong Raman peaks observed all other nanoparticles samples at 612 cm^{-1}, 774 cm^{-1}, 1089 cm^{-1}, 1364 cm^{-1}, 1509 cm^{-1}, and 1574 cm^{-1} were in good agreement with previous reports of R6G.[58] The SERS signal intensities from island like tiny Ag nanoparticles bound triangular Au nanoplates sample (Fig. 4e) shows largest enhancement compared to the other samples (Fig. 4a–d), with a R6G limit of detection of 1 μM. The SERS enhancement performance of the substrate can quantified according to previous works.[58,59] The prominent SERS band at 1574 cm^{-1} was selected for the calculation of enhancement factor (EF) by comparing R6G signals from bare silicon. The EF was calculated using the following equation.

$$EF = (I_{SERS}/I_{bulk})(N_{bulk}/N_{ads})$$

where I_{SERS} and I_{bulk} are the vibration intensity in the SERS and normal Raman spectra, respectively; N_{bulk} and N_{ads} are the number of molecules of solid and number of molecules of adsorbed R6G in the laser spot volume, respectively. N_{ads} is calculated from the following equation:

$$N_{ads} = N_d A_{laser} A_N/\sigma$$

where N_d is defined as the number density of tiny Ag nanoparticles on Au nanoprisms in the laser spot area (calculated as 140 ± 2 particles per μm^2), A_{laser} is the area of the laser spot (1 μm^2), A_N is the area of single tiny Ag nanoparticles on Au nanoprisms (calculated as ~34.6 × 10^{-4} μm^2), and σ is the area occupied by one R6G molecule (0.49 nm^2), respectively. Substituting all these calculated parameters, N_{ads} was estimated to be 9.88 × 10^5 molecules per μm^2. In our experimental conditions, the laser spot area and penetration depth were about 1 μm^2 and 15 μm, respectively. N_{bulk} of R6G was calculated to be 2.89 × 10^{10} using its density of 1.26 g cm^{-3}. The EF was calculated as 3.6 × 10^5, 6.9 × 10^5, 2.7 × 10^6, 7.1 × 10^6, and 4.3 × 10^7 for samples shown in Fig. 4a–e, respectively. The substantial Raman signal calculated from electromagnetic enhancement for molecules physically or chemically adsorbed to the metallic nanostructures depends on the surface morphology of the metal nanostructure substrate.[60] In this work, SERS enhancement not only depends on the inherent structures of triangular Au nanoplates (*e.g.*, sharp corners/tips) but also on the density of "hotspots" between adjacent tiny Ag nanoparticles. Such high density of "hotspots" arising from adjacent tiny Ag nanoparticles arranged in bunch of islands like structure on the triangular Au nanoplates plays an important role in SERS signal enhancement. Furthermore, the tiny Ag nanoparticles structures bound on entire active sites of triangular Au nanoplates, providing maximum "hotspot" for SERS enhancement compared to triangular Au nanoplates. In addition, the islands like structure of tiny Ag nanoparticles can easily capture the R6G molecules compared to the individual triangular Au nanoplates, which would efficiently improve SERS enhancement factor when compared to the other nanomaterials based SERS substrate (Table S1†).

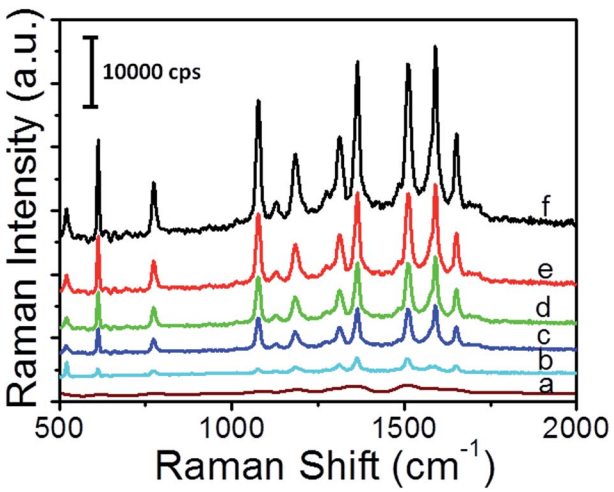

Fig. 4 SERS spectra of R6G obtained on the bare Si wafer (a), Au nanoplates (b), and Ag nanoparticles on Au nanoplates were shown in Fig. 3a–d, respectively (c–f). The SERS spectra were obtained with λ_{ex} = 633 nm excitation source.

4. Conclusions

We have prepared high density of tiny Ag nanoparticles bound triangular gold nanoplates by seeded growth method. The concentration of $AgNO_3$ and AA in the growth solution was the important key factor, which determined the formation of island like tiny Ag nanoparticles on the triangular Au nanoplates. We also demonstrated the advantage of this nanostructure as a SERS platform, towards the detection of R6G molecule, which is promising for further sensing and optical imaging applications.

Acknowledgements

We thank the Chinese Academy of Science for Hundred Talents Program, Chinese Central Government for Thousand Young Talents Program, the Natural Science Foundation of China (21404110, 51473179, 51573203), Ningbo Science and Technology Bureau (Grant 2014B82010 and 2015C110031), the

Technology Foundation for Selected Overseas Chinese Scholar, Ministry of Personnel of China (2015), School of Pharmacy, Fudan University & The Open Project Program (SDD2015-01) of Key Lab of Smart Drug Delivery (Fudan University), Ministry of Education, China.

Notes and references

1 M.-C. Daniel and D. Astruc, *Chem. Rev.*, 2004, **104**, 293–346.
2 Y. Huang, L. Wu, X. Chen, P. Bai and D.-H. Kim, *Chem. Mater.*, 2013, **25**, 2470–2475.
3 C. Gutiérrez-Sánchez, M. Pita, C. Vaz-Domínguez, S. Shleev and A. L. de Lacey, *J. Am. Chem. Soc.*, 2012, **134**, 17212–17220.
4 T. Maiyalagan, P. Kannan, M. Jönsson-Niedziolka and J. Niedziolka-Jönsson, *Anal. Chem.*, 2014, **86**, 7849–7857.
5 P. Kannan, J. Dolinska, T. Maiyalagan and M. Opallo, *Nanoscale*, 2014, **6**, 11169–11176.
6 G. Jiang, L. Wang, T. Chen, H. Yu and C. Chen, *Mater. Chem. Phys.*, 2006, **98**, 76–82.
7 J. Chen, P. Xiao, J. Gu, D. Han, J. Zhang, A. Sun, W. Wang and T. Chen, *Chem. Commun.*, 2014, **50**, 1212–1214.
8 Y. Huang, A. R. Ferhan, Y. Gao, A. Dandapat and D.-H. Kim, *Nanoscale*, 2014, **6**, 6496–6500.
9 Y. Huang, A. Dandapat and D.-H. Kim, *Nanoscale*, 2014, **6**, 6478–6481.
10 P. Kannan, T. Maiyalagan and M. Opallo, *Nano Energy*, 2013, **2**, 677–687.
11 Y. Huang and D.-H. Kim, *Nanoscale*, 2012, **4**, 6312–6317.
12 M. Grzelczak, J. Perez-Juste, P. Mulvaney and L. M. Liz-Marzan, *Chem. Soc. Rev.*, 2008, **37**, 1783–1791.
13 L. Scarabelli, M. Coronado-Puchau, J. J. Giner-Casares, J. Langer and L. M. Liz-Marzán, *ACS Nano*, 2014, **8**, 5833–5842.
14 M. L. Personick, M. R. Langille, J. Zhang and C. A. Mirkin, *Nano Lett.*, 2011, **11**, 3394–3398.
15 J. Grunes, J. Zhu, E. A. Anderson and G. A. Somorjai, *J. Phys. Chem. B*, 2002, **106**, 11463–11468.
16 S. E. J. Bell and N. M. S. Sirimuthu, *J. Am. Chem. Soc.*, 2006, **128**, 15580–15581.
17 D. Millo, F. Harnisch, S. A. Patil, H. K. Ly, U. Schröder and P. Hildebrandt, *Angew. Chem., Int. Ed.*, 2011, **50**, 2625–2627.
18 X. Yang, C. Gu, F. Qian, Y. Li and J. Z. Zhang, *Anal. Chem.*, 2011, **83**, 5888–5894.
19 L. Guo, G. Chen and D.-H. Kim, *Anal. Chem.*, 2010, **82**, 5147–5153.
20 P. Kannan, M. Los, J. M. Los and J. Niedziolka-Jonsson, *Analyst*, 2014, **139**, 3563–3571.
21 P. Si, Y. Huang, T. Wang and J. Ma, *RSC Adv.*, 2013, **3**, 3487–3502.
22 L. Guo, Y. Huang, Y. Kikutani, Y. Tanaka, T. Kitamori and D.-H. Kim, *Lab Chip*, 2011, **11**, 3299–3304.
23 V. P. Drachev, M. D. Thoreson, E. N. Khaliullin, V. J. Davisson and V. M. Shalaev, *J. Phys. Chem. B*, 2004, **108**, 18046–18052.
24 M. J. Banholzer, J. E. Millstone, L. Qin and C. A. Mirkin, *Chem. Soc. Rev.*, 2008, **37**, 885–897.
25 G. Kumari and C. Narayana, *J. Phys. Chem. Lett.*, 2012, **3**, 1130–1135.
26 S. P. Mulvaney, M. D. Musick, C. D. Keating and M. J. Natan, *Langmuir*, 2003, **19**, 4784–4790.
27 B. Yan, A. Thubagere, W. R. Premasiri, L. D. Ziegler, L. Dal Negro and B. M. Reinhard, *ACS Nano*, 2009, **3**, 1190–1202.
28 R. Wilson, S. A. Bowden, J. Parnell and J. M. Cooper, *Anal. Chem.*, 2010, **82**, 2119–2123.
29 K. Zhang, J. Zhao, H. Xu, Y. Li, J. Ji and B. Liu, *ACS Appl. Mater. Interfaces*, 2015, **7**, 16767–16774.
30 M. P. Cecchini, V. A. Turek, J. Paget, A. A. Kornyshev and J. B. Edel, *Nat. Mater.*, 2013, **12**, 165–171.
31 P. Ma, F. Liang, Q. Diao, D. Wang, Q. Yang, D. Gao, D. Song and X. Wang, *RSC Adv.*, 2015, **5**, 32168–32174.
32 P. Ma, F. Liang, Y. Sun, Y. Jin, Y. Chen, X. Wang, H. Zhang, D. Gao and D. Song, *Microchim. Acta*, 2013, **180**, 1173–1180.
33 P. Ma, F. Liang, D. Wang, Q. Yang, Z. Yang, D. Gao, Y. Yu, D. Song and X. Wang, *Dyes Pigm.*, 2015, **122**, 224–230.
34 J. Liang, H. Liu, C. Huang, C. Yao, Q. Fu, X. Li, D. Cao, Z. Luo and Y. Tang, *Anal. Chem.*, 2015, **87**, 5790–5796.
35 C. Kong, S. Sun, X. Zhang, X. Song and Z. Yang, *CrystEngComm*, 2013, **15**, 6136–6139.
36 X. Liu, L. Cao, W. Song, K. Ai and L. Lu, *ACS Appl. Mater. Interfaces*, 2011, **3**, 2944–2952.
37 S. K. Srivastava, A. Shalabney, I. Khalaila, C. Grüner, B. Rauschenbach and I. Abdulhalim, *Small*, 2014, **10**, 3579–3587.
38 J. Song, B. Duan, C. Wang, J. Zhou, L. Pu, Z. Fang, P. Wang, T. T. Lim and H. Duan, *J. Am. Chem. Soc.*, 2014, **136**, 6838–6841.
39 X. Liu, L. Zhao, H. Shen, H. Xu and L. Lu, *Talanta*, 2011, **83**, 1023–1029.
40 V. Joseph, A. Matschulat, J. Polte, S. Rolf, F. Emmerling and J. Kneipp, *J. Raman Spectrosc.*, 2011, **42**, 1736–1742.
41 W. Li, Y. Guo and P. Zhang, *J. Phys. Chem. C*, 2010, **114**, 6413–6417.
42 S. Lin, W. Zhu, Y. Jin and K. B. Crozier, *Nano Lett.*, 2013, **13**, 559–563.
43 S. Nie and S. R. Emory, *Science*, 1997, **275**, 1102–1106.
44 C. J. Orendorff, L. Gearheart, N. R. Jana and C. J. Murphy, *Phys. Chem. Chem. Phys.*, 2006, **8**, 165–170.
45 M. Fan, F.-J. Lai, H.-L. Chou, W.-T. Lu, B.-J. Hwang and A. G. Brolo, *Chem. Sci.*, 2013, **4**, 509–515.
46 M. Mandal, N. Ranjan Jana, S. Kundu, S. Kumar Ghosh, M. Panigrahi and T. Pal, *J. Nanopart. Res.*, 2004, **6**, 53–61.
47 P. Kannan, C.-S. Yoon, S.-C. Yi, S. Y. Lee and D.-H. Kim, *Mater. Chem. Phys.*, 2015, **156**, 1–8.
48 J. E. Millstone, S. Park, K. L. Shuford, L. Qin, G. C. Schatz and C. A. Mirkin, *J. Am. Chem. Soc.*, 2005, **127**, 5312–5313.
49 S. S. Shankar, A. Rai, B. Ankamwar, A. Singh, A. Ahmad and M. Sastry, *Nat. Mater.*, 2004, **3**, 482–488.
50 A. Miranda, E. Malheiro, E. Skiba, P. Quaresma, P. A. Carvalho, P. Eaton, B. de Castro, J. A. Shelnutt and E. Pereira, *Nanoscale*, 2010, **2**, 2209–2216.
51 Y. Qin, X. Ji, J. Jing, H. Liu, H. Wu and W. Yang, *Colloids Surf., A*, 2010, **372**, 172–176.

52 C. L. Haynes and R. P. van Duyne, *J. Phys. Chem. B*, 2003, **107**, 7426–7433.
53 S. Nah, L. Li and J. T. Fourkas, *J. Phys. Chem. A*, 2009, **113**, 4416–4422.
54 L. Bi, J. Dong, W. Xie, W. Lu, W. Tong, L. Tao and W. Qian, *Anal. Chim. Acta*, 2013, **805**, 95–100.
55 S. L. Kleinman, E. Ringe, N. Valley, K. L. Wustholz, E. Phillips, K. A. Scheidt, G. C. Schatz and R. P. van Duyne, *J. Am. Chem. Soc.*, 2011, **133**, 4115–4122.
56 A. B. Zrimsek, A.-I. Henry and R. P. van Duyne, *J. Phys. Chem. Lett.*, 2013, **4**, 3206–3210.
57 W. Nogala, P. Kannan, S. Gawinkowski, M. Jonsson-Niedziolka, M. Kominiak, J. Waluk and M. Opallo, *Nanoscale*, 2015, **7**, 10767–10774.
58 Y. Huang, A. R. Ferhan, S.-J. Cho, H. Lee and D.-H. Kim, *ACS Appl. Mater. Interfaces*, 2015, **7**, 17582–17586.
59 Y. Fang, N.-H. Seong and D. D. Dlott, *Science*, 2008, **321**, 388–392.
60 S. Sarkar, S. Pande, S. Jana, A. K. Sinha, M. Pradhan, M. Basu, J. Chowdhury and T. Pal, *J. Phys. Chem. C*, 2008, **112**, 17862–17876.